3D Scanning Technology as a Standard Archaeological Tool for Pottery Analysis: Practice and Theory

Avshalom Karasik and Uzy Smilansky

Department of Physics of Complex Systems, The Weizmann Institute of Science, Rehovot, 76100 Israel.

and

The Institute of Archaeology, The Hebrew University, Mount Scopus, Jerusalem, 91904 Israel.

Abstract

This article reports on the successful completion of a large-scale pilot project, where 3D scanning technology, and newly developed software to optimally identify the rotation axis of wheel produced ceramics, were used as a practical tool for pottery analysis. Approximately 1000 potsherds from several sites and periods were scanned, their symmetry axis computed, and their mean profiles drawn. The variety of fragments shapes, sizes and surface properties enabled us to test the system for a large range of archaeologically relevant pottery types. The high rate of success of the system, its efficiency and its output in the form of accurate, print quality profiles, encourage us to recommend this method as a practical and reliable tool in Archaeological research.

Keywords: 3D pottery analysis, rotation axis, automatic alignment, automatic drawing

I. Introduction

One of the most time consuming yet unavoidable tasks in Archaeology is the study of ceramic potsherds. These finds provide a considerable part of the archaeological information, and yet, it is exactly the abundance of the potsherds, (typically, thousands of indicative fragments per excavation season) which obstructs their detailed analysis. When the original vessels were axially symmetric, the potsherds can be completely characterized by their profiles. Extraction of the profile thus becomes the unavoidable first step in the analysis. Traditional methods for studying pottery, based on the slow and often inaccurate manual drawings, simply cannot handle the volume of information within reasonable time and cost [9,22,24: 89-93,26].

Various attempts to overcome these difficulties were proposed in the past, amongst which the use of a *profilograph* is a notable example [7]. The application of computerized, 3D scanning for pottery analysis was studied by several research groups [2,20,28,32,34]. While the 3D scanning technology has made impressive strides in the last decade, its applications as a practical tool to accompany and serve Archaeological projects, did not reach beyond its embryonic stage. One of the main obstacles is the lack of a reliable and efficient algorithm for the extraction of the symmetry axis and the subsequent drawing of a representative profile. This task is not trivial because several hurdles must be overcome:

- The fragments usually cover a rather small part of the full perimeter of the original vessel. The smaller the fragment, the harder it is to establish its correct positioning.
- The original vessels are usually not perfectly symmetric. On the macroscopic scale, they might be slightly deformed, or with the interior and the exterior

faces which are not exactly concentric. On the microscopic scale, the surfaces of ancient ceramics are rough either because of the production techniques and materials or because of weathering and breakage during the long time which elapsed between their production and the present. These irregularities suffice to destabilize positioning algorithms which work perfectly well for smooth surfaces.

- The 3D surface obtained from the scanner includes points which are not a part of the original surface of the vessel. Rather, they may belong to the *fracture surface* (which was generated when the original vessel was broken) or to surface defects, and their presence in the model is a nuisance which has to be systematically removed.

These problems are only marginally alleviated even if one limits the task to include only *indicative fragments* - the fragments which contain a part of the rim of the original vessel.

The earliest attempts to deduce the symmetry axis from the 3D scanner output were based on the observation that the vectors perpendicular to a perfect surface of revolution intersect at the axis. (The vectors of unit length which are perpendicular to a surface are referred to as the *normal vectors*). Thus, the line which minimizes the squared distances to the normal vectors defines the symmetry axis [3,13,27]. However, this method is very sensitive to outliers and to noisy data, and gets progressively unstable as the angle spanned by the fragment becomes small. The main reason for this instability is that extracting the normal vectors involves numerical differentiation, which is sensitive to noise – in the present context the noise is due to the roughness of the pottery surface and the finite spatial resolution of the scanners. The method can be used to provide an initial positioning, but more robust methods

should be used to approach the optimal axis [12,16]. Another observation was used to constrain the search for the optimal axis: the normal vectors from points which are equally far from the rim, coalesce at a single point on the symmetry axis. These points can be identified by the fact that their curvature eigenvalues are the same [4]. This constraint is introduced at the cost of having to compute the curvature tensor which requires the numerical computation of the second derivatives of the surface and the sensitivity to noise and outliers increases.

Being aware of the adverse effects of numerical differentiation in the presence of noise, several authors developed methods which do not involve quantities which depend on the normal vectors and their divergence [12,16]. Yao and Shao [37] compute the symmetry axis by detecting the 'corner points' of the rim, and finding the best fit of a circle to these points. Similarly, Kampel and Mara [16] identify circular patterns (rills) on the surface of the fragments and by using the fact that they represent concentric horizontal features they compute the symmetry axis as the line which joins the centers of the circles. Halir [12] makes use of the fact that in wheel produced ceramic, any horizontal section of a broken fragment is a circular arc. Thus, he uses an iterative scheme in which horizontal sections provide circular arcs whose centers provide an improved estimate of the axis. This algorithm is very efficient for surfaces which are parts of cylinders or cones, that is, for surfaces whose profiles consist of straight lines. However, for surfaces which are formed by the rotation of a more complex profile (e.g., archaeological potsherds) this method fails. The reasons for this failure will become clear after the method we use is explained in section III and in the mathematical appendix. When the fragment is well positioned the centers of the horizontal circular arcs, should meet at one point or form a small cluster. Therefore, Mara [21: 34-36] chose a strategy of searching for the alignment that would yield the

cluster with a minimal radius. This search is performed by systematically rotating the fragment in many directions and computing the corresponding centers of the horizontal sections. The position with the lowest standard deviation is chosen as a first guess. Then, two more similar iterations are done in the neighborhood of this guess in order to improve the results. This method may improve the robustness of the algorithm but increases dramatically the computation time. Moreover, there is no confidence that the final result is the optimal one since local minima may occur**.**

We tried to apply the known algorithms for the analysis of the Tel-Dor assemblage and did not get satisfactory results, due in large part to the rather small angles spanned by the fragments in this assemblage (see Figure 13 and the discussion in chapter IV). Hence, we were forced to develop a new algorithm which would be stable and efficient enough to ensure reliable analysis of our data. The present paper describes this method, and its test in a pilot project where ca. 1000 potsherds were scanned and analyzed. The potsherds were excavated in several sites in Israel - Tel Dor (814 fragments), Kefar-Hananya (91 fragments), Bir-Safadi, Abu-Matar and Azor (45 almost complete vessels), covering a rather diverse spectrum of periods, clays and technologies. The extracted profiles were digitally stored as print-quality drawings. They also form the data-base for computerized typology of the type we reported previously [9,33]. The successful completion of this project encourages us to propose 3D scanning technology as a useful and practical tool in Archaeology.

We should emphasize at the outset that at this stage of the work we consider only *axially symmetric* potsherds and defer the analysis of fragments with handles or spouts to a future report. Moreover, we shall treat only indicative fragments. Otherwise, there is no restriction on the fragments shape, size or surface.

The paper is organized in the following way. In the next chapter - *From potsherd to a triangulated point cloud* - we briefly describe the 3D-scanner, the scanning process and the setup we developed for a simultaneous scan of several (2-8) potsherds to shorten substantially the scanning stage. The following chapter - *From triangulated point cloud to a mean profile* - describes the algorithm which we constructed for finding of the axis of symmetry of potsherds. This step is crucial for any further analysis, and in particular for the extraction of the potsherds profiles. Special methods and quality tests had to be devised for the purpose, since the objects to be analyzed are broken fragments of complete vessels, often displaying a rough surface. We shall illustrate the process in action, and discuss in detail its range of applicability and possible pitfalls. Only the principles of our approach will be described, leaving all the mathematical and technical details to the appendix. The first trials of the new system will be the subject of the chapter *Applications.* Here we shall describe the assemblages of ceramics we have measured and analyzed. Based on the experience gained in these first large scale trials, we shall give a critical summary of the method, and outline possible future developments. The appendix - *Mathematical and technical details* - provides details on the computer algorithms developed for the purpose. It can be skipped by the practitioners who might not be interested in such details.

II. From potsherds to triangulated point clouds

In this chapter we shall share the experience we gained by the scanning of about 1000 potsherds, and provide several ways and means which we devised to accelerate the scanning procedure and further analyses.

The scanner and the setup: The 3D scanning camera produced by the firm *Polygon Technology*, Darmstadt, Germany[1], is based on the principle of structured light projected on the object and recorded by two digital cameras. The system shown in Figure 1 consists of a projector positioned between two cameras which are attached to a solid bar. The bar is mounted on a tripod. Each view of the object is recorded simultaneously by the cameras, and transformed to a 3D point cloud which represents the partial view.

The on-line analysis is performed by the control and evaluation program *QTSculptor*. In order to have the full image of the object, one has to scan it several times from different directions and register the scans together into one model. This is conveniently done by placing the object on a rotation table which is controlled by the software.

Figure 1: The scanning system: a solid bar mounted on a tripod holding a projector positioned between two cameras.

Placing the rotation table at a distance of approximately cm100 we get sufficient geometrical resolution, and a depth (and width) of view of order cm50.

[1] The scanner was purchased by the Zinman Institute of Archaeology at the Haifa University in collaboration with the Weizmann Institute of Science, and supported by ISF grant no. 727/05.

Since the bulk of our assemblage typically consists of fragments with size ranging between cm5-15 we can position several fragments with minimal mutual obstruction in this relatively large sensitive volume. This allows us to scan up to 8 fragments simultaneously thus increasing the scanning efficiency by a similar factor. In practice, the fragments are attached to a light metallic frame by clamps whose position in space can be adjusted (See Figure 2). A primitive version of such a frame, built from a wooden frame and "crocodile" connectors was tried by us during the 2004 Tel Dor excavation season [22,35]. The fragments are clamped to the holders such that their rims are approximately parallel to the axis of rotation of the table, and their surfaces are perpendicular to the plane of the frame. The number of fragments is only limited by the requirement that mutual shadowing is avoided. The bar which carries the projector and the cameras is now set vertically, so that it is parallel to the rotation axis of the table. In this way the light pattern on the fragments can be seen by the two cameras, offering the best conditions for extracting the 3D information. Typically, 6-10 exposures taken with the table angles at 60^0-36^0 intervals, respectively, suffice for an accurate and complete 3D reconstruction. It is clear that the upper and lower sides of the potsherds are badly exposed, and the clamps also show in the reconstructed surface. However, because of the way the fragments are attached to the frame, the eliminated portions of the potsherd consist mainly of the fracture surfaces. The rim and the bulk of the fragment surface are not affected. This is a price worth paying for achieving high scanning efficiency – typically, 60 fragments can be scanned per hour! This high rate of scanning was routinely achieved by a single operator who worked with two frames: one frame being loaded with fresh fragments, while the other is scanned. This high rate reflects the minimum "on line" time required by the scanner.

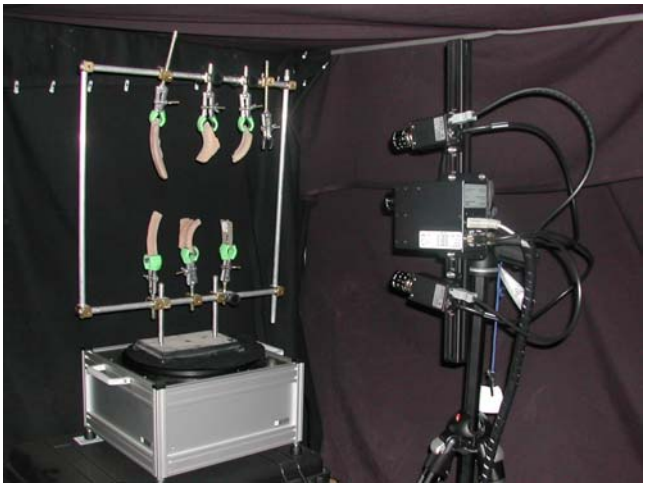

Figure 2: The scanning system (right) and a frame, with 6 fragments attached to it, standing on the rotation table.

Creating the 3D model as a triangulated point cloud: After scanning, the views have to be combined (registered). The resulting point clouds should be separated to several files – a file for each fragment. The *QTSculptor* program performs these tasks interactively with the operator. There are three crucial tasks which the operator has to perform: 1. To separate the volumes where each of the fragments is to be found, and remove the parts of the images which show the clamps. 2. To mark a reference grid on each of the fragments. 3. To keep track of the identity of the fragments and associate the correct file names to the corresponding fragments. Even though the *QTSculptor* is user friendly, and gets the instructions by clicks on the mouse, this part of the work takes time, and slows down the processing rate. If this stage of the work were performed by the scanning operator between successive scans, the rate would be reduced to approximately 10-15 fragments per hour. However, one can achieve a much higher rate by employing two operators who work simultaneously with separate computers.

The output of the scanning stage consists, for each fragment, of a triangulated cloud map which resides in a reference frame. For the further analysis the operator

chooses the reference (*x*,*y*) plane by marking three points on what she/he considers as defining the rim plane or any other plane parallel to the rim. This plane is used as a first approximation for the determination of the symmetry axis of the fragment. Figure 3 shows a "framed" potsherd with the (*x*,*y*) plane tangent to the rim.

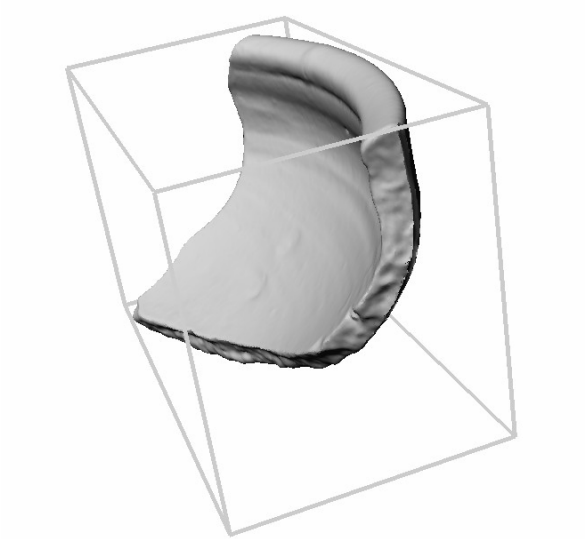

Figure 3: A bowl fragment from Tel Dor and its initial positioning in a reference coordinate system. The rim plane is approximately parallel to the upper face of the bounding-box.

III. From triangulated point cloud to a mean profile

As was mentioned before, the most efficient way to store the information on pottery fragments of wheel-produced vessels is in term of their profiles - the cross-sections with planes which go through the symmetry axis. The profiles are indispensable components for any further archaeological analysis, such as typological classification or comparisons. The importance of the correct identification of the axis of rotation is repeatedly emphasized in many Textbooks for Archaeology [11: 51-58,15: 423,24: 173,29: 222] - false positioning may lead to ridiculous misinterpretations. To emphasize this point we show in Figure 4 three drawings which were produced using the same profile which was aligned at three different angles with respect to the assumed axis. This suffices to represent three totally different vessels.

An experienced archaeologist may exclude the wrong positioning. Here, when we seek to develop an automatic computerized alignment, we depend entirely on the algorithm to find the correct position of the potsherds.

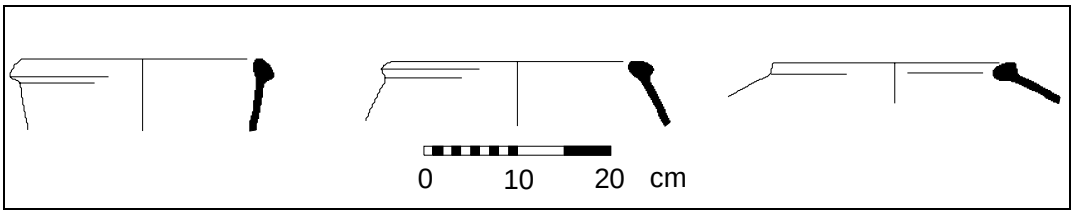

Figure 4: An identical profile tilted to three different angles and shown as a standard drawing in an archaeological report. The different drawings represent three different archaeological types. This illustrates the absolute importance of the correct alignment for further analysis and interpretation.

The position of a potsherd is determined once the axis of symmetry of the original vessel is known. To define an axis uniquely one must specify two angles θ and φ which determine the orientation of the axis (see Figure 5) and the anchor-point $\mathbf{b} = (b_x, b_y)$ in the (*x*,*y*) plane. The computer algorithm reorients and shifts the axis until a satisfactory positioning is determines.

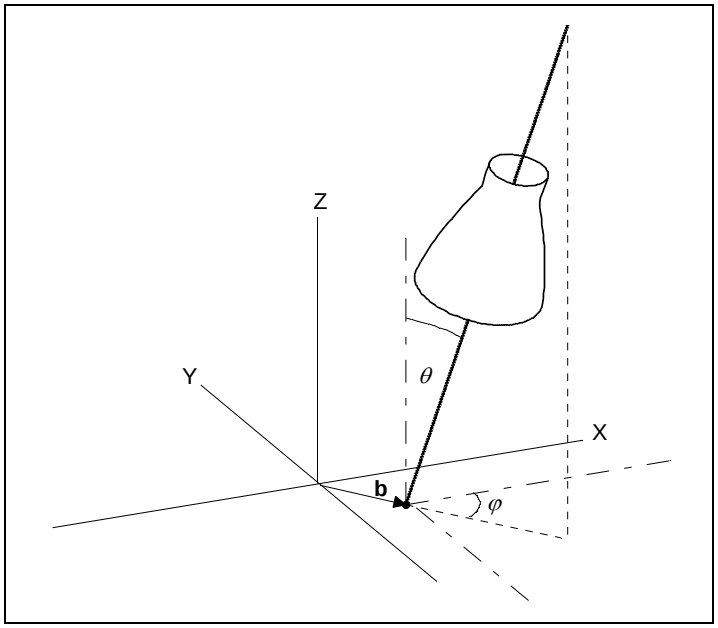

Figure 5: The parameters which define the axis position relative to the fixed reference frame.

We start the description of our algorithm by explaining how the concept of "optimal positioning" is defined in a quantitative way. Given an axially symmetric body, all the points which are at the same height h along the symmetry axis are at the same distance ρ from the axis. Plotting h *vs.* ρ for all the points on the surface, one gets a line which is the profile of the vessel (see Figure 6-b). This operation projects the points of the vessel to a single plane – the reference plane. However, if the assumed axis is not the true axis, the points in the reference plane form a thick line which gets thicker as the assumed axis is further away from the true axis (see Figure 6-a). At each point *s* on the line we can determine the width of the line *q(s)*, which for convenience, we express as a percentage of the mean wall thickness of the fragment. The mean width of the projected profile (obtained as the average value of *q(s)* taken along the profile) provides a quantitative measure of the quality of the assumed axis. We define therefore the *quality factor*:

$$Q = 100 \frac{mean\ \ width\ \ of\ \ projected\ line}{mean\ \ wall\ thickness\ of\ \ fragment} .$$

The purpose of the algorithm is to determine the axis which minimizes *Q*. More details about the quality factor and its computation in practice are provided below and in the Appendix. Figure 6 illustrates the action of the algorithm by showing two projected profiles of the same potsherd plotted before and after the proper axis was computed. The shift of the anchor point was computed to be 10mm and the orientation changed by $\Delta\theta = 4.5^0$. The *Q* value was improved from the initial value *Q*=12.39 to *Q*=2.47.

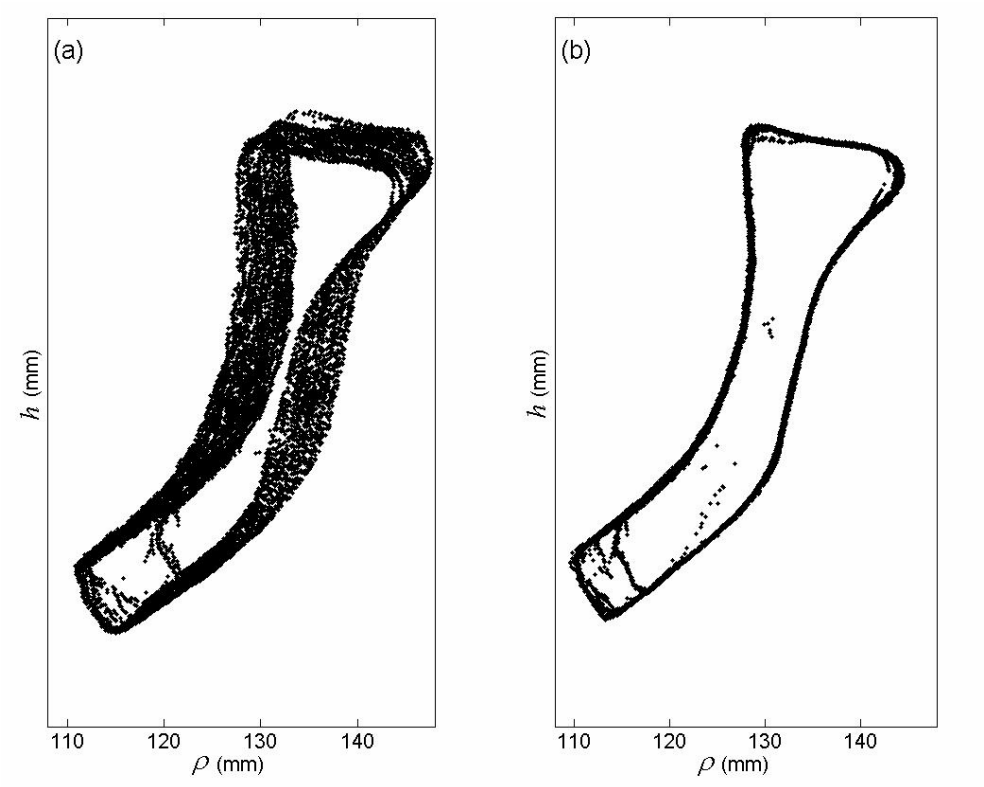

Figure 6: The projected profile for a fragment from Tel Dor before (a) and after (b) positioning.

If the surface were an exact surface of revolution, the projected profile would converge to a strict geometrical curve, and Q would vanish at perfect positioning. However, the method used to exclude fracture surfaces and other defects has a finite tolerance and not all the points which deviate from axial symmetry are filtered out. Moreover, the surface might be slightly deformed, on either the macroscopic or microscopic scale. Both effects set an intrinsic minimum value to the projected line thickness and hence to Q. The numerical value of Q depends also on the mean fragment thickness. Thus, Q is most helpful to gauge the improvement in positioning of the *same* fragment, and it is less reliable as a tool to compare the quality of the positioning of *different* fragments.

To compute the quality factor in practice, we proceed by intersecting the projected profile with thin adjacent rectangles (See Figure 7). The rectangles are oriented perpendicular to the line, and are sufficiently long to cover it transversally.

The width of each rectangle varies from point to point on the projected profile within a given range, and is inversely proportional to the mean curvature at the point. For each of the rectangles we compute the center of mass of the points within the rectangle (gray points in Figure 7). The local width *q(s)* of the projected line in the *s* rectangle is obtained by computing the variance of the transversal distances of the points from the tangent to the line through the center of mass.

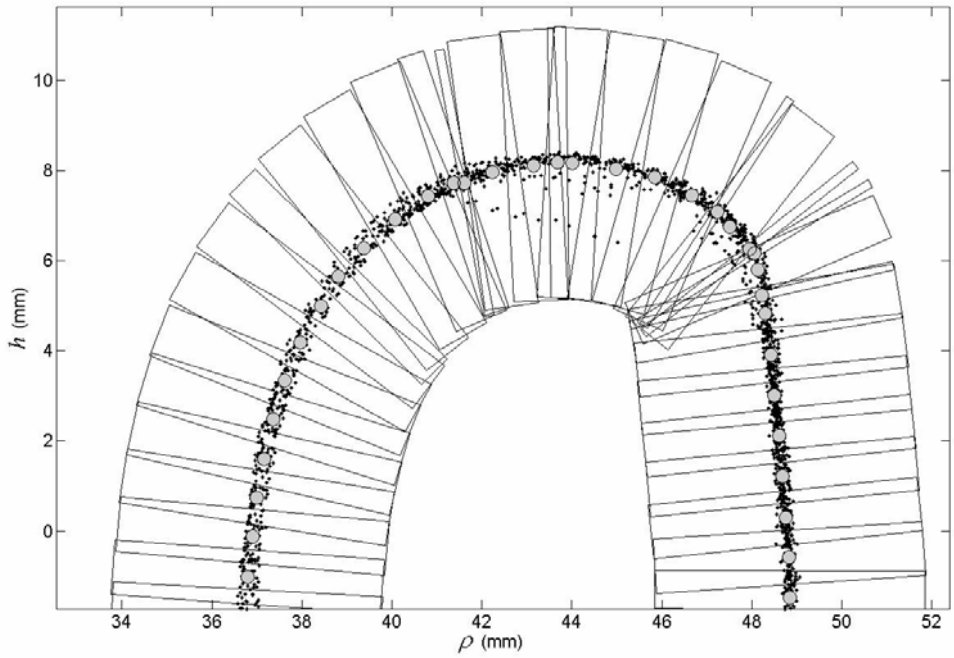

Figure 7: The projected profile and the rectangles used to determine its thickness.

We shall describe below the method which optimizes the positioning, and show how it overcomes the problems which are met in practice. In the present discussion we shall refrain from technical issues, which are deferred to the Appendix.

It is assumed at the outset that the operator who scanned the fragment already positioned it in an approximately correct way as explained above. Thus, a first approximation of the symmetry axis can be computed. The next step consists of removing the points which belong to the fracture surfaces and to other surface defects. We make use of the fact that for each of the triangles formed by adjacent points on the

surface, one can compute a vector which approximates the normal to the surface. The normal vectors to a surface of revolution intersect the axis of rotation. Vectors normal to the fracture surfaces or to other features which violate the assumed axial symmetry do not have this property. This fact is used effectively to eliminate the irrelevant parts of the scanned surface. This is illustrated in Figure 8 which compares the projected points of the entire vessel (b) to the points which were selected according to the directions of their normal vectors (c).

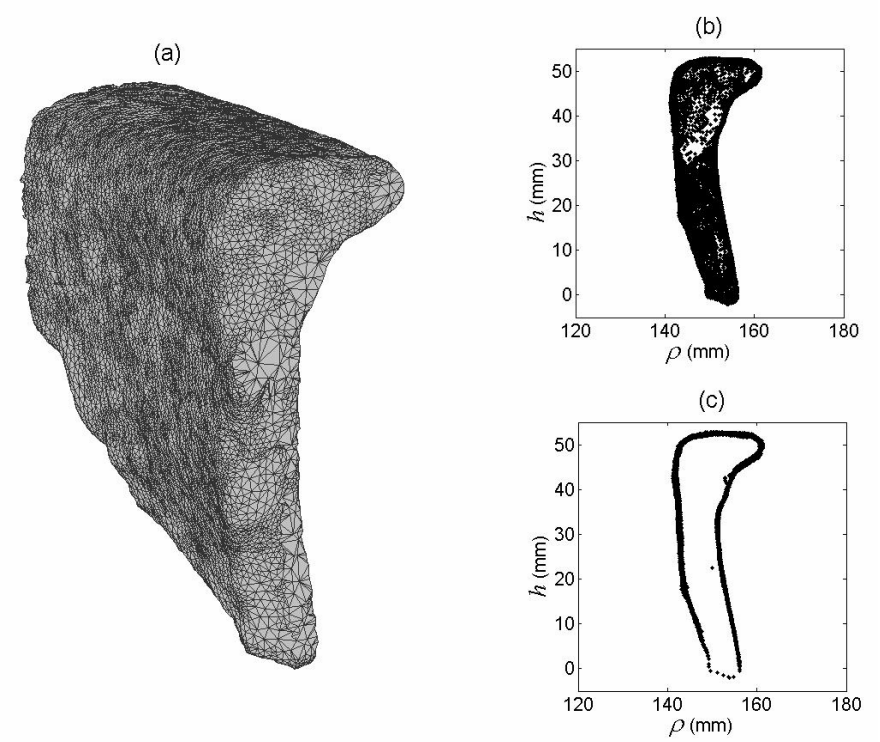

Figure 8: *(a)* A 3D model of a well positioned ceramic piece from Tel Dor. (*b*) The projected points on the reference plane, no selection applied. (*c*) Projected points selected by the criterion that the normal vectors point in the approximate direction of the symmetry axis.

Our method of positioning emulates and generalizes the traditional method which is based on placing the rim on a planar plate such that the contact between the rim and the plate is maximal. The plate then defines the tangent plane which is parallel to the plane of the original wheel. The vessel symmetry axis is perpendicular to the tangent plane, and goes through the center of the arc generated by the contact

points of the rim with the table. If we intersect the vessel with any other plane which is parallel to the tangent plane, we would find two *concentric* circles (or arcs when we deal with fragments), and their common center lies on the axis of rotation. Thus, by cutting the 3D representation of the vessel by several parallel planes, we can identify the axis of rotation as the line which goes through the centers of the concentric circles. The tangent to the rim is just a special case of this family of planes - the one where the two circles, corresponding to the inner and outer surfaces, coalesce to a single circle. Because of the special role and properties of the rim, our algorithm which is based on the above understanding, consists of two independent steps. The first, endeavors to find the axis of rotation as the line of centers of the circular arcs which result from the planar intersections. We shall refer to this method as the *horizontal sections method*. The second makes use of the points of the rim, and attempts to find the best fitting plane tangent to the rim. This method will be referred to as the *rim-tangent method*. The horizontal sections method takes advantage of the entire information on the surface and therefore it is usually more stable and reliable. The rim-tangent method is used for fine tuning, and it improves the quality factor in some cases.

The horizontal sections method can be best explained by the following consideration. Assume that the fragment is aligned such that its axis coincides with the z - axis (the "vertical" axis) of a reference system of coordinates (this reference coordinates system is fixed once for all and is not changed during the search of the symmetry axis). Next, the fragment is intersected by horizontal planes, their number depends on the fragments size, and is typically in the range 60-100. The centers of the circles traced by the sections are computed. The center points are then vertically projected on one horizontal plane. If the approximate axis coincides with the true axis, the points

on the reference plane converge to a point which is the anchor point of the axis on the reference *(x,y)* plane. It can be shifted to the origin of the reference coordinate system, and the alignment procedure is successfully terminated. Due to the roughness and deformations of the surface, and also because of the finite resolution, the projected points might form a small cluster, and then the anchor point is determined by their center of gravity (see the lower right frame in Figure 9). During the alignment process, however, the approximate axis is tilted with respect to the true axis, and the projected center points form a line segment (see the lower center frame in Figure 9). The direction of the line provides the information necessary to obtain an improved alignment. The computer program emulates this line of thinking in an iterative procedure which is repeated until no further improvement can be achieved. The convergence of the line to a very small cluster is illustrated in the second row of Figure 9 which shows also the corresponding *Q* values and the projected profiles. Here we used a smooth and perfectly symmetric surface of revolution and therefore the center points could be made to converge to an exceedingly small cluster. (Note the change of scale as the positioning improves – from millimeter to micrometers!). The mean radius of the cluster reflects the uncertainty (accuracy) of the resulting alignment. This procedure turns out to be stable, fast and it provides accurate determination of the axis, even in the presence of microscopic and macroscopic deformations. The axis determined by the horizontal sections method, is used as a first guess in the algorithm which implements the rim-tangent method.

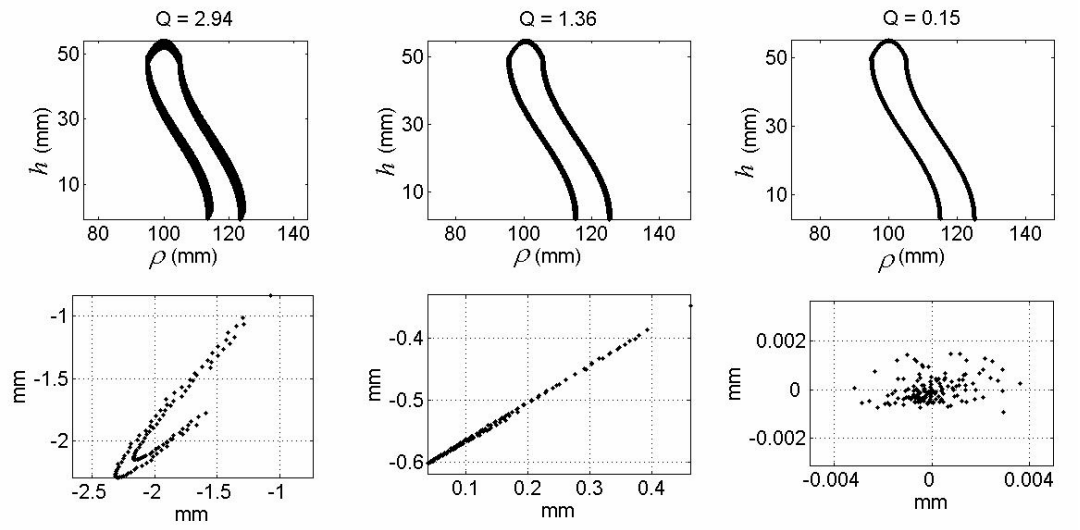

Figure 9: Three stages in the alignment procedure of a fragment of a smooth and perfectly symmetric surface: The columns (left to right) represent the initially tilted positioning, after a single iteration and the final, converged positioning. The first row shows the *projected profiles* and the second row the clustering of the centers of the horizontal sections (note the scale difference at successive columns).

The rim-tangent method consists of the following steps. Given an approximate symmetry axis, the fragment is intersected vertically by a fan of planes which go through the axis. The fragments trace profiles on the planes, and the coordinates of the highest point of each profile are recorded. The new estimate of the tangent to the rim is the plane which goes optimally through the maximum points. The normal to this plane gives the improved axis direction. The anchor point is given by the center of gravity of the centers of the horizontal sections as in the former method. In many cases the application of the rim-tangent method improves the *Q* factor as illustrated in Figure 10. Here, the thickened rim was better preserved and it represents a larger part of the perimeter than the body, which is relatively broken. The rim-tangent method improves the alignment, and *Q* is reduced from 3.62 to 2.15.

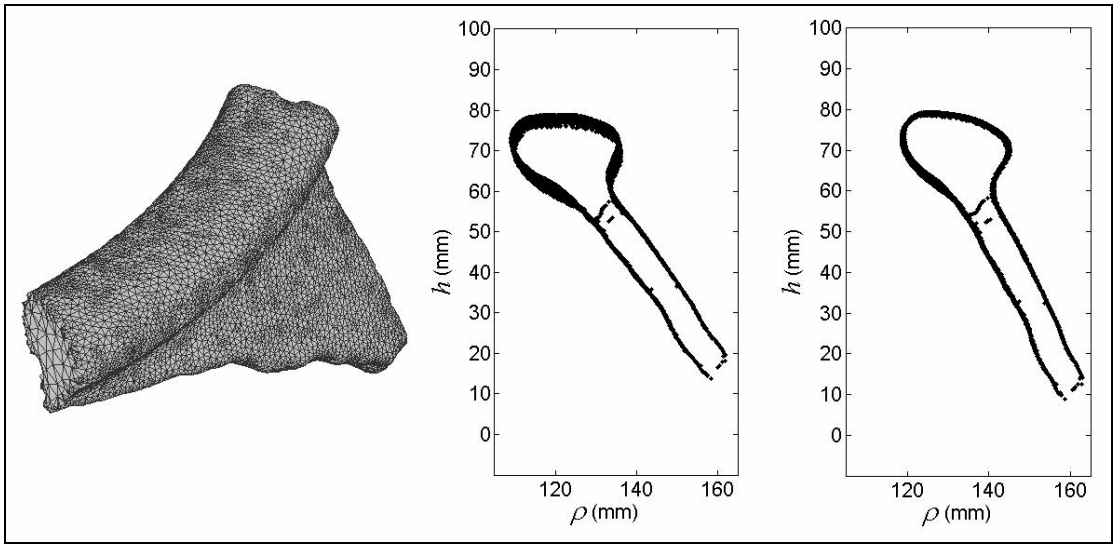

Figure 10: The improvement in the projected profile by the rim-tangent method: The 3D model of the fragment from Tel Dor is shown (left) with the original stage of its projected profile at the end of the horizontal sections method (center), in comparison to the profile improved by the rim-tangent method (right).

The quality or accuracy of the alignment of a potsherd was defined above as the percentage ratio between the mean width of the projected profile and the mean wall thickness of the potsherd. *Q* is computed after each iteration, and the process is satisfactorily ended when convergence is achieved and *Q* reaches below a prescribed value $Q_{\max}$. In this case the file is transferred to the 'successful' folder. However, if convergence is not reached within 10 iterations or if the process converged to $Q > Q_{\max}$, a warning flag is raised and the file is transferred to the 'failures' folder. The actual value of $Q_{\max}$ has to be determined empirically for each assemblage, depending on its specific characteristics, such as surface roughness, the mean thickness *etc*.

Examining the local width along the profile can provide interesting insights about the potsherd. The lower row in Figure 11 shows the local width functions *q(s)* for 3 different fragments which are optimally aligned. The corresponding *projected profiles* are shown in the upper row. The exterior surface of the left fragment in

Figure 11 is less rough, which is expressed by the relatively lower values of *q(s)* in the corresponding interval (1-50). The arrows (marked by 1 and 2) indicate two places where points which belong to the fracture surface were not deleted. Their effect on the local width function is shown by the two peaks in the lower left plot (marked by two arrows respectively). However, it is important to note that the influence of these peaks on the final *Q* value is very small, since there are very few of them. Similarly, in the right fragment of Figure 11, a distortion at the middle of the interior part is indicated by arrow 3. This can be detected by the corresponding high values of *q(s)* in the vicinity of $s = 130$. This sensitivity of *q(s)* to local details along the profile might be useful in future applications.

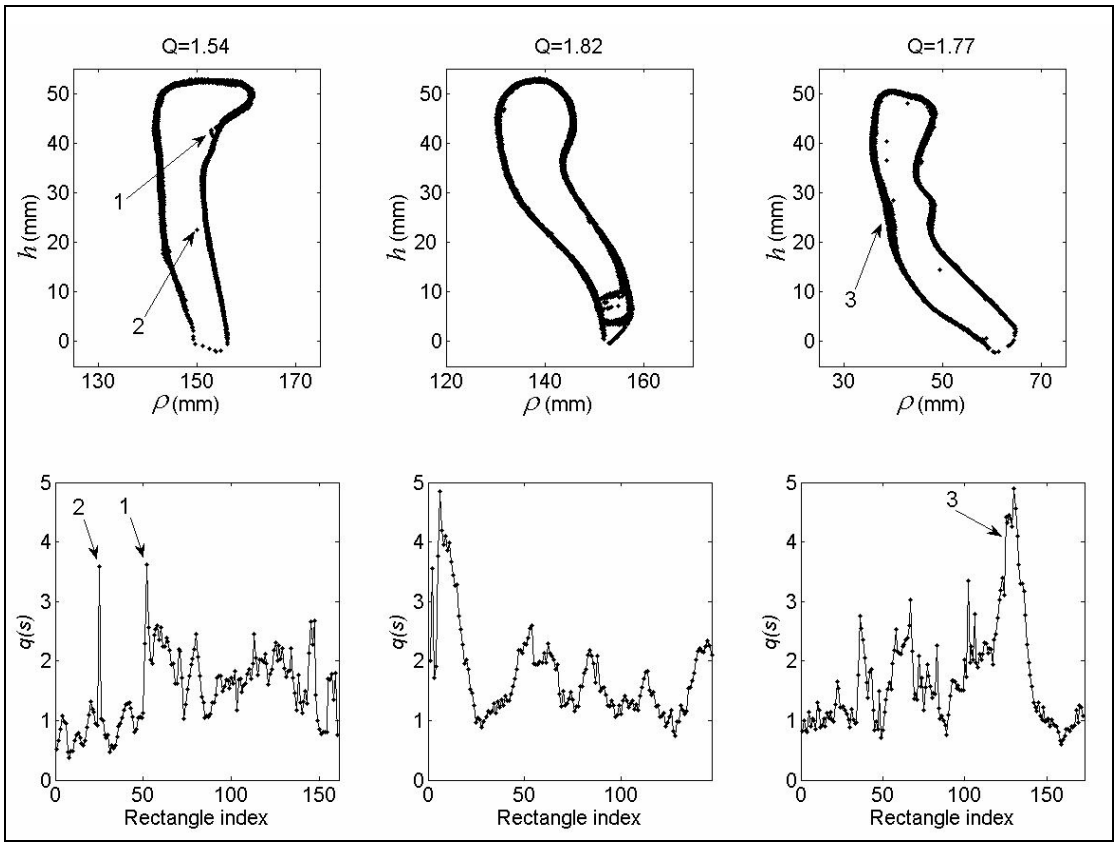

Figure 11: The projected profiles of three different potsherds from Tel Dor, and the corresponding distributions of the widths within the rectangles (bottom). The points along the profiles are arranged counter clock wise, starting at the lower point of the exterior (bottom right).

Once the optimal alignment is found, the center points of the rectangles provide also the mean profile which characterizes the potsherd for further documentation and analysis. This definition touches upon a methodological question which is at the basis of the study of ceramics, namely, which single profile should be used in order to represent a given fragment. This is a question one must face especially when dealing with slightly deformed, rough and not evenly fractured potsherds. As long as the profile is drawn manually, the artist integrates the entire information and produces a drawing which reflects his/her judgment. When a 3D scan is available, one could use the longest profile as a representative [17] or another single cross-section which is the closest to the average shape [14; here they use a different definition for the average]. Due to the fact that single profiles may be affected by local, non representative deformations, and the recognition that the entire surface of the fragment stores the information about the profile, we prefer to introduce the concept of the "mean profile" as described above. It uses the entire information available, it excludes local details and small deformations and it does so without bias.

The mean profile is also used for the final drawings of the potsherd in the standard format used in published archaeological reports (see Figures 12 and 17). According to convention, a mirror symmetric, complete section is drawn with the symmetry axis represented by a line. The right side is blackened, and the line of the rim orifice is shown. On the left side only the exterior part of the profile and the rim are plotted. Carination and wheel-marks are also illustrated with horizontal lines, their lengths being proportional to the local curvature of the profile. These features are drawn automatically, based on the analysis of the profile curvature without the operator's intervention.

IV. Applications

This chapter reports on three studies in which ceramic assemblages from the southern Levant were scanned and evaluated. This is the ultimate test of the system, and it enabled us to judge the reliability and assess its rate of success in practice. Of particular importance is the critical discussion of those (few) potsherds which the method failed to evaluate. A detailed discussion of these cases will end this section.

The assemblages used for this study span a wide range of periods, from Chalcolithic via the Iron-Age to Roman and early Byzantine, and they cover quite optimally the range of features and difficulties expected to be encountered in future archaeological studies.

The Assemblages:

1. Tel Dor - The main and the largest collection consists of 814 early Iron Age potsherds from Tel Dor [10,36]. This assemblage is a complete set of *indicative* fragments from one stratigraphical horizon. It is a typical Iron-Age assemblage in the coastal Levant, consisting mainly of house-ware vessels for daily use.

2. Kefar-Hananya - The second group counts 91 bowl fragments from Kefar-Hananya which were all categorize by the excavator as belonging to a single type [type 1E, 1: 103-109]. This site has a long tradition of pottery production over more than 400 years during the Roman and the early Byzantine periods. We used this assemblage also to compare our algorithm to another method in which the fragments are drawn by computerized *profilograph*, where the positioning was manually done by an Archaeologist.

3. Chalcolithic v-shape bowls – The last assemblage consists of 45 complete *v-shape* bowls from various Chalcolithic sites in the southern Levant [5,6,8,25]. It is believed that these early vessels were shaped with the aid of simple wheels [30,31], and indeed

they are rough and deviate from perfect axial symmetry. Since the vessels are complete, the optimal symmetry axis can be computed unambiguously. However, the quality measure can differ substantially from the previous assemblages, because of the surface roughness and deformations, which enables the study of the correlation between the quality factor and the production technology.

Each of these assemblages will now be discussed in detail.

Tel Dor – The scanning of this assemblage was our first project with the Polygon 3D scanner and software. Out of the scanned indicative 814 potsherds, 760 were successfully positioned and their profiles extracted. They were checked visually by an experienced archaeologist and all passed successfully his scrutiny. This group of fragments comprises of a large variety of shapes, sizes, surface qualities and deformations. It gave us the opportunity to test our system to its limits. We shall first discuss this group of fragments. The remaining 54 "failures" will be discussed subsequently. Figure 12 shows computer drawings of a few typical examples of the shapes and sizes in the "successful" assemblage.

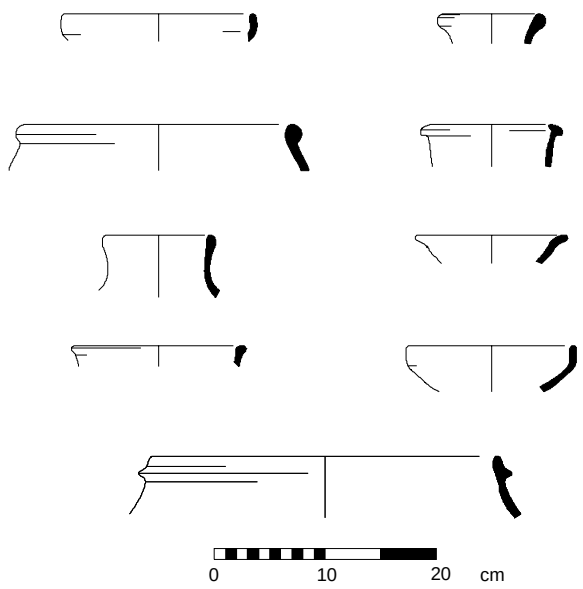

Figure 12: Several Iron-Age potsherds from Tel Dor. The print quality drawings were produced by the computer program without the operator's intervention.

The most important limiting factor for a successful computer positioning is the size of the fragment compared to the circumference of the original vessel. This is further exacerbated by the surface roughness and deformations of archaeological finds. Expressing the rim size in degrees (a complete rim extends 360^0), we show in Figure 13 the distribution of the angular sizes of the Tel Dor potsherds which were successfully positioned and analyzed. Most fragments extend angles smaller than 35^0, which correspond to less than 10% of the rim circumference. In a recent publication which refers to this issue, a threshold value of 25^0 is mentioned as the minimum angular size for successful automatic alignment of potsherds [21]. Our method for fragments positioning, handled successfully 208 fragments rims in the range 13^0 -25^0 - a substantial proportion of the assemblage.

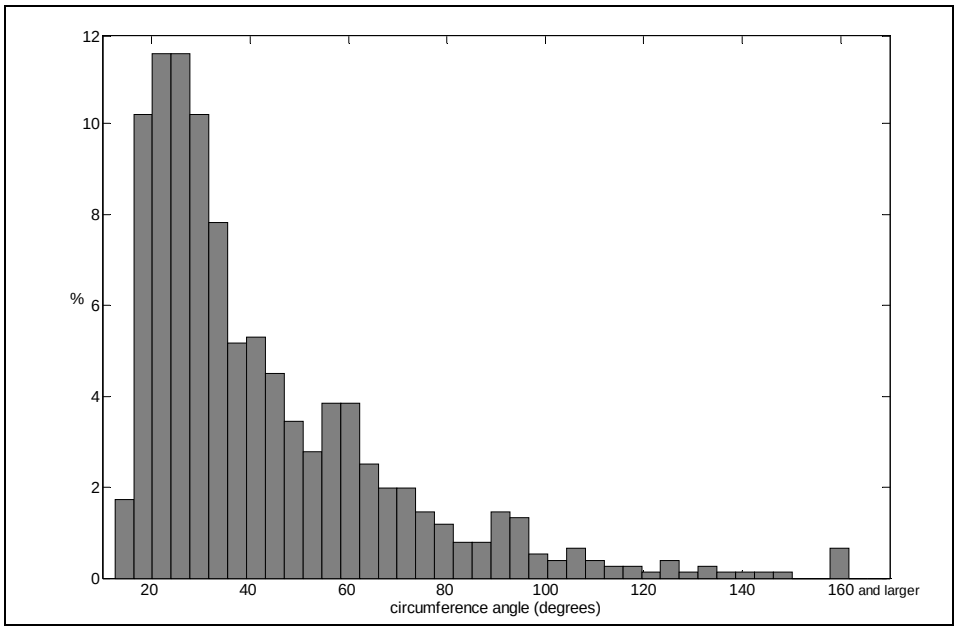

Figure 13: The distribution of the rim circumference for the Tel Dor assemblage.

The distribution of the quality factor Q is shown in Figure 14. We found empirically, that in the analysis of the Tel Dor assemblage, satisfactory positioning is usually achieved when $Q < Q_{\max} = 4$. The fragments which satisfy this condition were

stored in the “successful” folder. All others were stored in another folder and required further scrutiny. Higher Q values are not necessarily due to faulty alignment. For instance, in some fragments, the automatic selection and deletion of the points on the fracture surfaces (see Figures 8, 11), is not as successful. Similarly, protrusions, rough surfaces and also handles will have the same effect. We chose to pay special attention to cases with $Q \geq 4$ just as a matter of caution.

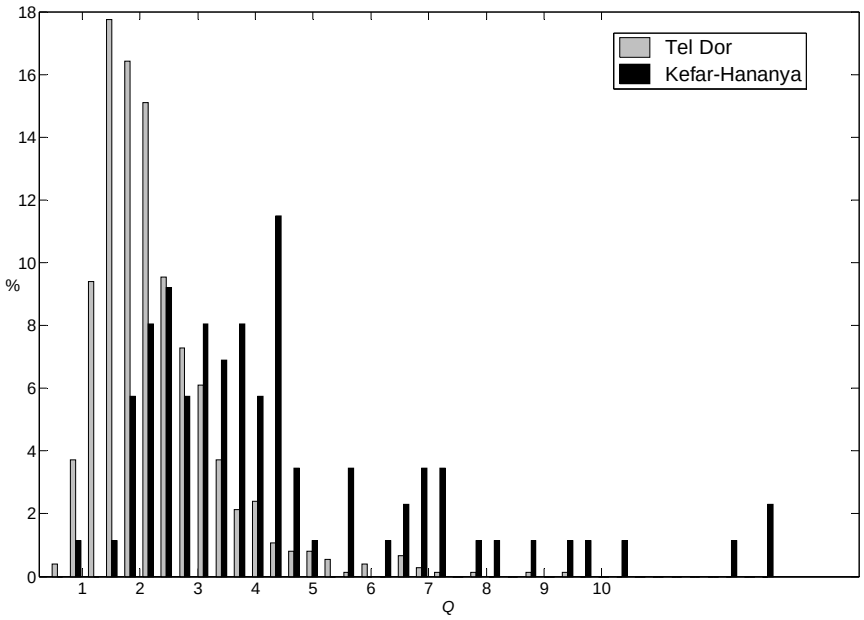

Figure 14: A comparison of the distributions of Q for the assemblages of Tel Dor and Kefar-Hananya.

After the first run of the analysis was completed the potsherds in the 'failures' folder was further scrutinized. Those files for which the projected profiles deemed acceptable, in spite of their relatively high Q values, were transferred to the 'successful' folder. The remaining 54 potsherds for which the alignment algorithm failed can be partitioned as follows:

Small perimeter arc: (15 potsherds) The angular range of these potsherds is 9.5^0-25^0 with 11 pieces with less than 15^0, which barely overlaps with the angular range where successful positioning was registered. The distinction between these groups is not sharp because the perimeter length is not the only factor which determines the success

of the positioning. Rather, it is very much dependent on the roughness and deformation of the fragment.

Macroscopic deformations: (28 potsherds) Large deformations of the type shown in figure 15, violate the assumption which is at the basis of the method, namely, that the fragments are parts of an axially symmetric vessel. These fragments were included in the assemblage only because their deformation was not detected by the operator.

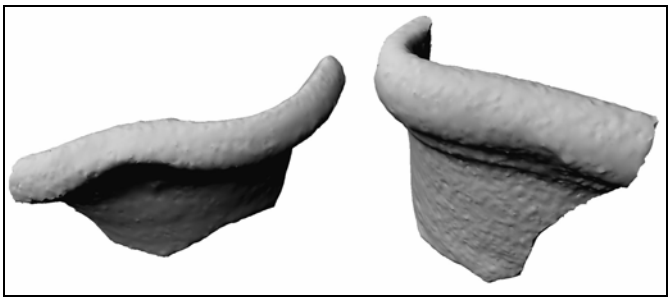

Figure 15: Two models of deformed fragments from Tel Dor which violate axial symmetry could not be automatically positioned.

Flat potsherds: (11 potsherds) As will be explained in the appendix, fragments with significant flat parts violate an assumption implicit in the algorithm concerning the rate of change of the distance between a point on the surface and the symmetry axis, as a function of the height along the symmetry axis. Two examples of such fragments are shown in Figure 16, one is a jar with a rim area consisting of a small and short neck on relatively large and mostly horizontal shoulder (see Figure 16 right) and the other is a flat tray with no neck at all (Figure 16 left). As long as the fragment is not exclusively of this type, and has other parts which are not flat parts, the positioning is successful. However, this is not always the case, and indeed in the Tel Dor assemblage 1.3% of the fragments were classified as flat examples.

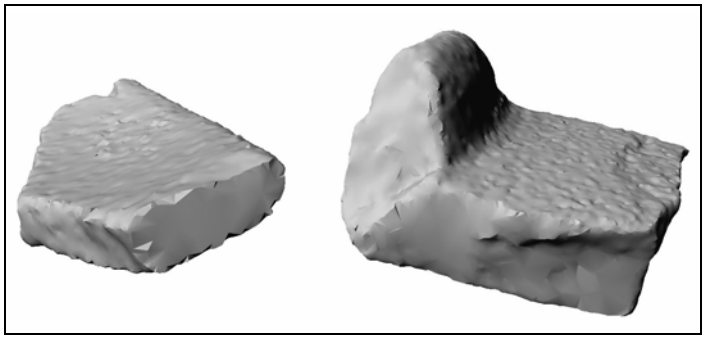

Figure 16: Two models of potsherds from Tel Dor with significant flat parts for which the algorithm failed. Left - a piece of a flat tray ; Right - a fragment of a jar with short neck and horizontal shoulder.

2. Kefar-Hananya – This assemblage consists of fragments which were defined as belonging to the same type (bowl 1E) by the excavator [1, see Figure 17]. No further selection criterion was imposed. The fragments originate from two different production centers at the same site.

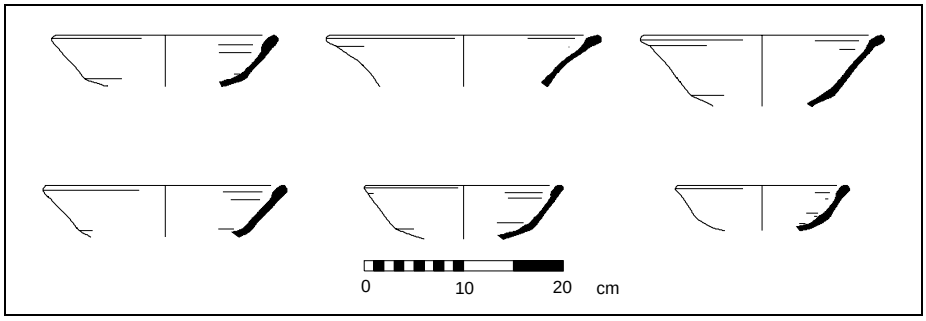

Figure 17: Type 1E bowls from Kefar-Hananya, three from each production center (corresponding to the two rows of the Figure). The print quality drawings were produced by the computer program without the operator's intervention.

Out of the 91 potsherds only 4 were declared as failures because they were too small. Figure 14 shows the distribution of the *Q* value of the Kefar-Hananya assemblage. It is significantly higher than the *Q* distribution of the Tel-Dor assemblage, but this does not necessarily imply that the positioning is less certain or less accurate. Much of this increase is due to the fact that type 1E is a relatively thin vessel, and since we use the thickness for normalization of *Q*, the *Q* distribution is shifted to higher values. This demonstrates again that *Q* is best used for following the

improvement in alignment, and is not designed for comparative studies. Similarly, it illustrates the reason for setting $Q_{\max}$ individually for each assemblage. At the same time, one should keep in mind that the Kefar-Hananya vessels are kiln wasters that were dumped by the potters. One cannot exclude the possibility that these vessels were discarded because of minor deformations, which also affect the *Q* parameter.

As mentioned before, the Kefar-Hananya bowls were drawn also by a *profilograph* [7]. The fragments were positioned by the archaeologist and a single profile was followed using a computerized position-sensitive pointer. The radius was computed as the best fitted circle to a set of points that the operator marked on one horizontal plane (usually the rim or a parallel horizontal feature). Although, the resolution of the profile and the accuracy of the radius cannot compete with those of the 3D scanner, a comparison between the profiles obtained by the two methods is valuable, since the positioning in the *profilograph* is based on the experience of a well trained archaeologist who is familiar with the assemblage and the period. Figure 18 compares profiles of six vessels which were drawn both with the *profilograph* and with our algorithm following scanning. In most cases, the alignments of the two methods are very similar, which reinforces the archaeological confidence in the automatic procedure. However, the radii show larger deviations as can be seen in the lower row of Figure 18. This reflects a well known problem endemic to the *profilograph*. In a preliminary test using a different 3D acquisition system during the 2004 excavation season at Tel Dor, similar comparisons were performed [22]. However, the matching between the automatic alignment and the archaeologically based *profilograph* alignment was not satisfactory. This discrepancy motivated us to develop the system described in the present paper.

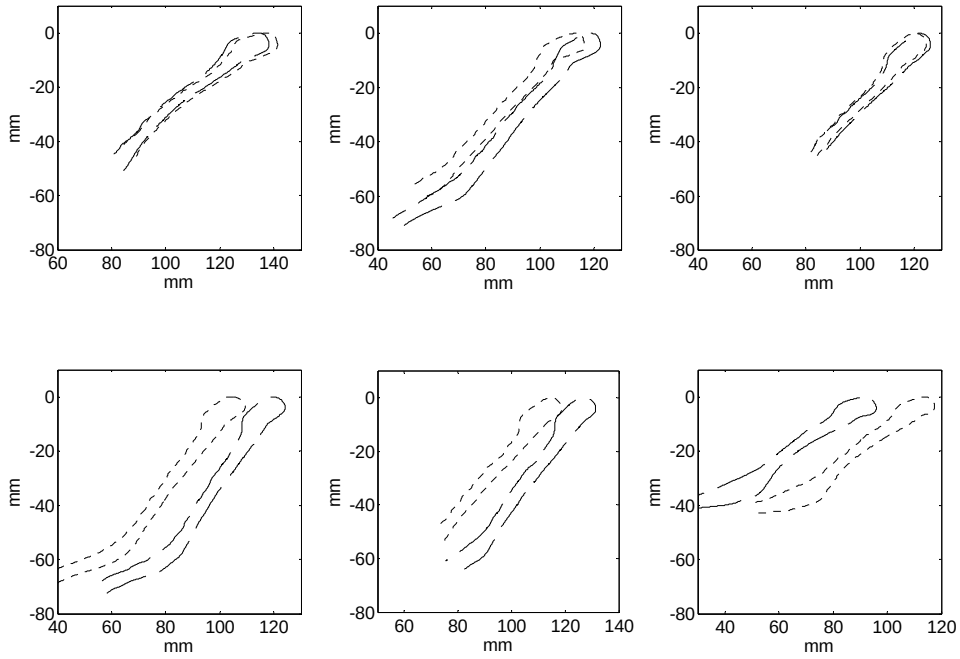

Figure 18: A comparison of six profiles from Kefar-Hananya which were drawn using the *profilograph* (dotted lines), and the mean profiles of the same fragments as defined by our algorithm (dashed lines).

3. Chalcolithic v-shape bowls – This assemblage consists of complete or nearly complete vessels known as *v-shape* bowls, which are characteristic to the Chalcolithic period in the southern Levant [8: 206-276]. Many of the obstacles that challenge the positioning algorithm when dealing with fragments are not relevant when complete vessels are studied. The computations of the best fitted circles are less sensitive to noise and to the fracture surfaces. Most of the alignment methods that are known in the literature will succeed here. However, when the vessel suffers macroscopic deformations, a representative profile cannot be well defined since the projected profile fills a thick and often blurred strip. In extreme situations the border between the points of the inner and outer surfaces of the vessel overlaps, as can be seen in the upper part of Figure 19. This is contrasted with the projected profiles obtained for a bowl produced on a modern fast-wheel shown at the lower part of the figure.

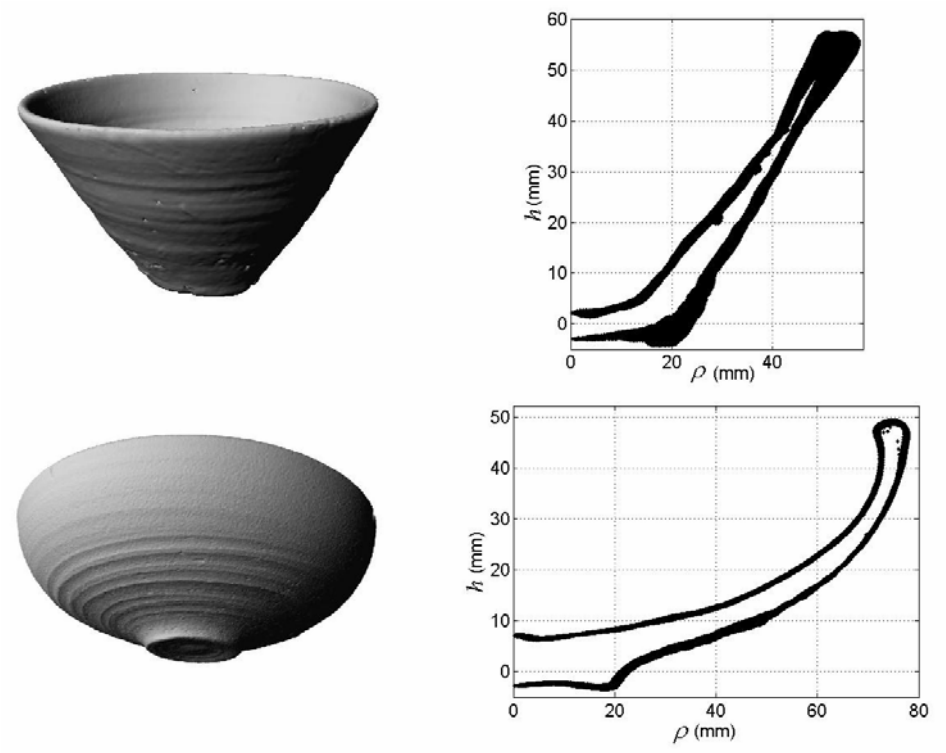

Figure 19: Projected profiles of a complete *v-shape* bowl from Bir-Safadi [top right, 6], and a modern bowl produced on a fast-wheel (bottom right). The corresponding 3D models are shown to the left.

Obviously, there is no single profile that can be chosen to represent the shape of the *v-shape* bowl. However, the macroscopic deformations can be well followed by producing profiles which represent small sectors along the vessel. This is shown in Figure 20 where we have plotted 10 profiles for each of the bowls, and each profile represents the mean projected profile of a 36^0 section of the complete circumference. The overlap of the profiles is much better for the modern bowl than for the *v-shape* one. Moreover the edges of the projected profile of each section were much clearer so that the parameter Q could be computed. The mean Q value for the various sections of the *v-shape* bowl was 3.50 with standard deviation of 0.58, in comparison to 1.06 and 0.22 (respectively) for the modern bowl.

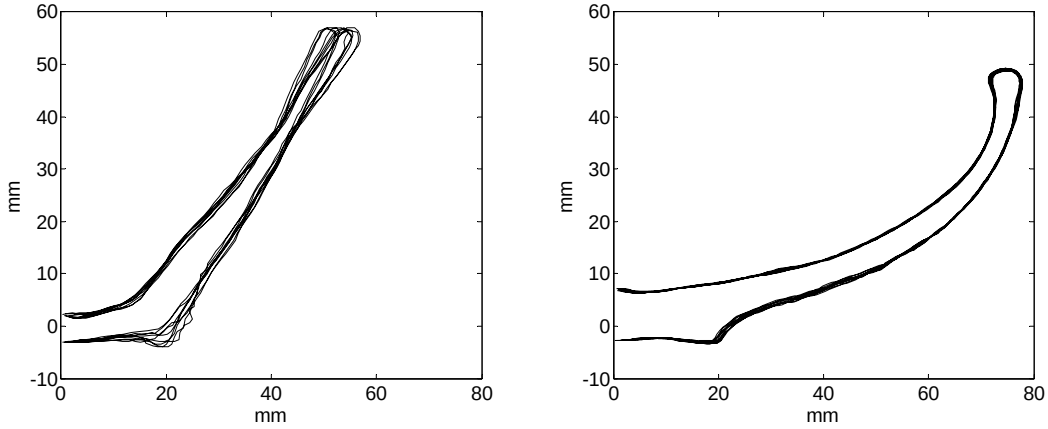

Figure 20: The overlap of 10 mean profiles for 10 equal sections of the *v-shape* bowl (left), and of the modern bowl (right).

Studying the section profiles enable us to discuss in a quantitative way the degree of deformation of the vessel. This idea, which was developed in [18,19,23,33] enables us to detect differences between production technologies such as e.g., differences in the speed of the wheels, expecting that the use of a slower wheel makes it more difficult for the potter to shape the clay in a uniform way.

V. Summary

In this paper we presented a new system for the study of pottery which is based on commercial 3D scanning hardware and software, and, on specially developed methods and computer algorithms which were specifically designed for the archaeological applications. We described the tests of this system on a large number of fragments (approximately 1000) and we believe that it is indeed a viable tool which has the potential of substantially improving the archaeological study of pottery. Several advantages are gained:

a. Small fragments can be scanned at the rate of 500 potsherds per day (8 hours) by a single operator. Training a student to operate the system takes 2-3 days.

At this rate, the scanned output consists of computer files which have to be further evaluated to produce the final point cloud models. This task can be carried out either offline, or, if it is done after each scanning by the same operator, the rate reduces to approximately 100 potsherds per day. Comparing to manual drawings which are produced at the rate of 15-20 per day, this is a major improvement.

b. The positioning algorithm proved to be robust and stable as long as the fragment covers more than 15^0 of the original circumference, and it does not consist mainly of a flat surface. The resulting positioning were scrutinized and approved by an expert archeologist. The success rate was higher than 90%.

c. The system offers diagnostic tools to test cases where a failure flag was raised.

d. The computed profiles are stored in digital form and converted easily to print quality drawings which can be added directly to the archaeological report.

e. The digitized profiles can be used directly as the input for further typological and comparative work, unlike manual drawings which have to be scanned.

f. The system can be also used as a tool for novel archaeological applications by studying e.g., the deformations of vessels and using them to unravel the technological reasons for their appearance.

Further developments are pending, and they include the analysis of non-indicative fragments and fragments which carry handles or spouts. Work on these extensions is in progress.

The authors will be ready to share the know-how and computer algorithm with any archaeologist who is interested to use this promising technology.

Acknowledgements

We would like to thank Ilan Sharon, Ayelet Gilboa and David Adan-Bayewitz, for their interest and constructive criticism during all the stages of this work, and also to express our gratitude for allowing us to use Archaeological material prior to its formal publication. We are grateful to Talia Goldman and Leore Grosman for their support, interest and comments on the manuscript, and to Rinat Bar-Hay for the *profilograph* measurements on the Kefar-Hananya assemblage. The Israel Antiquities Authority is acknowledged for providing the assemblage of the *v-shape* bowls. Support from the Kimmel Center for Archaeological Sciences at the Weizmann Institute, and the ISF grant 168\06 is acknowledged with thanks. U.S. is indebted to the Isaac Newton Institute and Clare Hall, Cambridge, for their hospitality while this paper was written, and acknowledges support from the EPSRC grant 531174.

Appendix: Mathematical and technical details

The appendix is intended for the readers who are interested in the more mathematical – algorithmic aspects of the present work, and it requires some basic knowledge of mathematics. The material is divided to several rather independent sections addressing different parts of the algorithm.

A.1 The algorithm for the optimal alignment of pottery fragments –

Our method is an iterative procedure, in which the position of the symmetry axis is successively improved, and the improvement is assessed by the quality factor *Q*. As was discussed previously, the initial orientation is provided by the operator of the scanner, who marks three points on what she/he deems as the plane of the fragments rim. The *QTSculptor* software assigns its coordinate system such that the rim plane is the (x, y) plane, and the *z*-axis is perpendicular to the plane, anchored at

the estimated center of the circle defined by the three reference points. This system of coordinates is kept fixed as a reference frame throughout the entire computation. At each iteration step the fragment is shifted and oriented such that the improved estimate of the symmetry axis coincides with the *z*-axis of the reference coordinate system. Each iteration starts by filtering away points on the surface which correspond to parts of the surface which do not belong to the original surface of the vessel (fracture surfaces) as explained in section III.

At each iteration four parameters determine the amount by which the fragment should be repositioned (Figure 5): two angles for the orientation, and two shift coordinates of the anchor point (the z coordinate is immaterial since changing it is equivalent to measuring the height on the symmetry axis relative to a different reference point). The repositioning of the fragment is carried out by the following basic operations

1. Rotate by an angle φ about the x-axis.
2. Rotate by an angle θ about the z-axis.
3. Shift by b_x along the x-axis.
4. Shift by b_y along the y-axis ($b_z = 0$)

A point on the surface, with coordinates $\mathbf{r} = (x, y, z)$ will have the new coordinates $\hat{\mathbf{r}} = (\hat{x}, \hat{y}, \hat{z})$ after the fragment is shifted and reoriented, with $\hat{\mathbf{r}} = T\mathbf{r} + \mathbf{b}$ and:

$$T = \begin{bmatrix} \cos\varphi & \sin\varphi & 0 \\ -\sin\varphi\cos\theta & \cos\varphi\cos\theta & -\sin\theta \\ -\sin\varphi\sin\theta & \cos\varphi\sin\theta & \cos\theta \end{bmatrix} \quad ; \quad \mathbf{b} = \begin{bmatrix} b_x \\ b_y \\ 0 \end{bmatrix}$$

The surface is assumed to be a surface of revolution. Suppose that after the transformation, the axis of symmetry coincides with the *z*-axis of the reference frame.

Then, per definition, the distance $\rho = \sqrt{\hat{x}^2 + \hat{y}^2}$ between a point on the surface and the symmetry axis is a function of $\hat{z}$ only. This function is the profile function which we denote by $f(\hat{z})$. Thus, in the new positioning of the fragment, $\rho^2 = f^2(\hat{z}) = |\hat{\mathbf{r}}|^2 - \hat{z}^2$. Our task can be stated in the following way:

Given a fragment whose profile function is unknown, and whose symmetry axis is aligned along an axis which deviates from the *z* axis of the reference frame, find the parameters $b_x, b_y, \theta, \varphi$ of the transformation which will bring the symmetry axis to coincide with the *z*-saxis of the reference frame.

The horizontal sections method is based on the following observations:

Assume that the shift and orientation parameters (b_x, b_y, θ) are small (no assumption regarding φ is necessary). Consider the intersections of the surface with *N* planes parallel to the (x, y) plane, which are defined by the points of intersection of each of the planes with the *z* axis in the reference system $z = z_i,\ i = 1,...,N$. Then, to leading order in the parameters (b_x, b_y, θ):

i. The intersection of the plane $z = z_i$ with the fragment surface comprises of two circular arcs, obtained by the intersection with the interior surface and the exterior surfaces of the fragment.

ii. Denote the coordinates of the centers of the circles in the (x, y) plane by $(\delta x_i, \delta y_i)_{\text{int}}$ and $(\delta x_i, \delta y_i)_{ext}$, where the subscripts stand for the interior and the exterior circles, and *i* denotes the index of $z = z_i$. The centers of the interior and exterior circles, for all the planes, converge to a straight line $\delta y_j = A\delta x_j + B$ where *j=1,…,2N* so that *j* goes over the interior and

exterior circles in the N planes. Moreover, $\varphi = \cot^{-1}(-A)$ and

$$b_x = -B\cos\varphi = -B\sqrt{\frac{\cos^2\varphi}{\cos^2\varphi + \sin^2\varphi}} = \frac{AB}{\sqrt{1+A^2}}\,.$$

iii. The following relations are satisfied:

$$b_y - [z_j + f(z_j)\cdot f'(z_j)]\cdot\theta = \delta x_j \cdot \sin\varphi - \delta y_j \cdot \cos\varphi \quad ; \quad j = 1,...,2N\,.$$

Knowing φ and b_x from *ii.*, the equation above determines b_y and θ by best fit.

The lower middle frame in Figure 2 shows how the points $(\delta x_j, \delta y_j)$ converge to a line. The plot to its left is obtained in the first iteration, where the assumption that the deviations are small is not satisfied. Still, a best fit to a straight line provides enough information to start the iterations in the correct way. The plot to its right shows the final coordinates of the circle centers. The points converge within a small radius showing that the symmetry axis of the fragment coincides with the *z*-axis to within a micrometer.

To prove the validity of the three points above, we start with the relation $f^2(\hat{z}) = |\hat{\mathbf{r}}|^2 - \hat{z}^2$ which must hold if the fragment symmetry axis coincides with the *z*-axis. To leading order in (b_x, b_y, θ)

$$|\hat{\mathbf{r}}|^2 = |T\mathbf{r} + \mathbf{b}|^2 = |\mathbf{r}|^2 + 2(\mathbf{b}T\mathbf{r}) + |\mathbf{b}|^2 \approx |\mathbf{r}|^2 + 2(\mathbf{b}T\mathbf{r})\,,$$

and therefore,

$$\begin{aligned} f^2(\hat{z}) &= |\mathbf{r}|^2 + 2(\mathbf{b}T\mathbf{r}) - \hat{z}^2 = \\ &= |\mathbf{r}|^2 + 2(x[b_x\cos\varphi - b_y\sin\varphi] + y[b_x\sin\varphi + b_y\cos\varphi] - z\,b_y\,\theta) - \hat{z}^2 \\ &= |\mathbf{r}|^2 + 2(x[b_x\cos\varphi - b_y\sin\varphi] + y[b_x\sin\varphi + b_y\cos\varphi] - zb_y\theta) \\ &- z^2 - 2z\theta(-x\sin\varphi + y\cos\varphi). \end{aligned}$$

We used above $\hat{z}^2 \approx z^2 + 2z\theta[-x\sin\varphi + y\cos\varphi]$. Since $|\mathbf{r}|^2 = x^2 + y^2 + z^2$ we can write,

$$f^2(\hat{z}) = x^2 + y^2 + \alpha x + \beta y + \gamma \tag{1}$$

with

$$\alpha = 2[b_x\cos\varphi - b_y\sin\varphi] + 2z\theta\sin\varphi$$
$$\beta = 2[b_x\sin\varphi + b_y\cos\varphi] - 2z\theta\cos\varphi$$
$$\gamma = 2z\,b_y\,\theta\,.$$

Using Taylor expansion we write,

$$f^2(\hat{z}) = f^2(z+\delta z) = f^2(z) + 2f(z)f'(z)\cdot\theta[-x\sin\varphi + y\cos\varphi] \tag{2}$$

By combining (1) and (2) we get:

$$f^2(z) + 2f(z)f'(z)\cdot\theta[-x\sin(\varphi) + y\cos(\varphi)] = x^2 + y^2 + \alpha x + \beta y + \gamma \tag{3}$$

For a given $z = z_j$, equation (3) describes a circle centered at $(\delta x_j, \delta y_j)$ where

$$\delta x_j = -(b_x\cos\varphi - b_y\sin\varphi) - z_j\theta\sin\varphi - f(z_j)\cdot f'(z_j)\cdot\theta\sin\varphi \tag{4}$$

$$\delta y_j = -(b_x\sin\varphi + b_y\cos\varphi) + z_j\theta\cos\varphi + f(z_j)\cdot f'(z_j)\cdot\theta\cos\varphi \tag{5}$$

Equation (3) proves observation *i.* above. Multiplying equation (4) by $\cos\varphi$ and adding to equation (5) multiplied by $\sin\varphi$ we get

$$\delta x_j\cdot\cos\varphi + \delta y_j\cdot\sin\varphi = -b_x \tag{6}$$

which proves observation *ii.*

Finally, multiply equation (4) by $\sin\varphi$ and subtract from it equation (5) multiplied by $\cos\varphi$ to get

$$\delta x_j\cdot\sin\varphi - \delta y_j\cdot\cos\varphi = b_y - z_j\theta - f(z_j)\cdot f'(z_j)\cdot\theta$$

and after rearranging the equation we get:

$$b_y - [z_j + f(z_j)\cdot f'(z_j)]\cdot\theta = \delta x_j\cdot\sin\varphi - \delta y_j\cdot\cos\varphi \tag{7}$$

which proves *iii.*

In practice, we use typically *N*= 60-100 horizontal sections. The number of equations exceeds the number of unknowns so that the parameters $b_x, b_y, \theta, \varphi$ are obtained by best fit. The profile function $f(z)$ and its derivative $f'(z)$ are computed iteratively from the mean projected profile deduced in the previous iteration. This is the only point in the computation where a numerical derivative is used. Still, the function $f(z)$ depends on a single parameter so the computation does not involve partial differentiation as is the case with the computation of the normal vectors and the curvature tensor.

Equation (7) is valid only when $|f'(z)|$ is bounded. This is not the case when the vessel has flat sections parallel to the (x, y) plane. Flat sections of this type are removed by the algorithm from the analysis, but if the fragment consists predominantly of such surface, the method fails. This explains the failure of the algorithm for the small flat fragments discussed in section IV.

The rim-tangent method is based on the observation that the symmetry axis of a wheel produced vessel is perpendicular to its orifice plane. As in the previous method, we use an iterative procedure to compute the necessary shift and alignment parameters $b_x, b_y, \theta, \varphi$ that should bring the symmetry axis to coincide with the *z*-axis of the reference system. Given an approximate positioning, vertical sections are defined as the intersections of the fragment with *M* vertical planes which fan out from the *z*-axis, and are separated by an angle of typically 2^0-3^0. The highest points in each section with coordinate vectors $\mathbf{r}_m = (x_m, y_m, z_m)$ are identified and stored. The set of M maximal points $\mathbf{r}_m$ represent the rim, and by realigning the fragment such that the plane tangent to the rim is perpendicular to the *z*-axis we obtain the improved

alignment. After realignment the maximal points will have the coordinates $\hat{\mathbf{r}}_m = (\hat{x}_m, \hat{y}_m, \hat{z}_m)$ which can be written as above (assuming θ is small):

$$\hat{\mathbf{r}}_m = T\mathbf{r}_m = \begin{bmatrix} x_m \cos\varphi + y_m \sin\varphi \\ -x_m \sin\varphi + y_m \cos\varphi - \theta z_m \\ -x_m \theta \sin\varphi + y_m \theta \cos\varphi + z_m \end{bmatrix}$$

Suppose that after the transformation the symmetry axis is brought to coincide with the *z*-axis, so that the $\hat{z}$ coordinate of all maximal points should be equal, and can be arbitrarily set to be zero. From which we get,

$$-x_m \theta \sin\varphi + y_m \theta \cos\varphi + z_m = 0 \ , \qquad \text{for every } m=1,...M \tag{8}$$

Minimizing the sum $\sum_{m=1}^{M} (x_m \theta \sin\varphi - y_m \theta \cos\varphi + z_m)^2$ with respect to the parameters $a_1 = \theta \sin\varphi$ and $a_2 = \theta \cos\varphi$, we get $\varphi = \tan^{-1}\left(\frac{a_1}{a_2}\right)$ and $\theta = \frac{a_1}{\sin\varphi}$.

The b_x, b_y parameters are calculated as the mean of all the centers of the best fitted circles to the arcs of the horizontal sections. The iterations are repeated until no improvement in *Q* is achieved.

A.2 The surface tensor and its principal axes –

Given a surface Ω, we denote by $\mathbf{n}(\mathbf{r})$ the outward pointing normal to Ω at the point $\mathbf{r} \in \Omega$. In our analysis we often encounter the question, what is the direction $\mathbf{h}$ which is parallel to the largest fraction of the normal vectors on Ω ? Two simple examples will suffice: Consider a complete vessel whose surface is a perfect surface of revolution. The corresponding $\mathbf{h}$ is the direction of the axis of symmetry, because this is the only direction to which there is a group of normal vectors all pointing to the same direction - the normals on the rim and the base (if it is flat). Moreover, the normal vectors on the rest of the vessel are distributed uniformly which selects the

main direction to be the mean normal to the base and the rim. For a small potsherd, the surfaces are almost planar, and $\mathbf{h}$ points in the direction of their mean normal. The normals to the rim have less weight, and the fracture surfaces will have minimal weight since the normals there point in arbitrary directions.

To find $\mathbf{h}$ in practice we have to maximize the mean projection of $\mathbf{h}$ on the normal vectors $\frac{1}{|\Omega|}\sum_{\mathbf{r}\in\Omega}|\mathbf{n}(\mathbf{r})\cdot\mathbf{h}|^2$ ($|\Omega|$ is the number of surface points) subject to the condition that $\mathbf{h}$ is of unit length. Using the Lagrange multiplier method, we have to find the extremum of the quadratic form,

$$\chi(\mathbf{h}) = \frac{1}{|\Omega|}\sum_{\mathbf{r}\in\Omega}|\mathbf{n}(\mathbf{r})\cdot\mathbf{h}|^2 - \lambda|\mathbf{h}|^2 .$$

Requiring that the first variation of $\chi(\mathbf{h})$ vanishes, we find that $\mathbf{h}$ must satisfy $T\mathbf{h} = \lambda\mathbf{h}$, where the tensor T is expressed explicitly as the 3x3 (symmetric) matrix,

$$T_{\alpha,\beta} = \frac{1}{|\Omega|}\sum_{\mathbf{r}\in\Omega} n_\alpha(\mathbf{r}) n_\beta(\mathbf{r}) \quad ; \quad \alpha,\beta \in (x,y,z)$$

There are in general 3 independent eigenvectors, corresponding to the 3 eigenvalues λ of *T*. The eigenvector with the largest eigenvalue is the vector which is parallel to the largest fraction of normals. This vector is referred to as the *principal normal*. It is attached to the point (not necessarily on the surface) $\frac{1}{|\Omega|}\sum_{\mathbf{r}\in\Omega}\mathbf{r}$. The other two eigenvectors identify local extrema of the quadratic form $\chi(\mathbf{h})$, and they might be of use in some applications. Figure 21 shows the surface of a typical potsherd with the field of normals attached. The eigenvectors are also shown at the right side of the Figure by thickened lines. Their length is proportional to the eigenvalues. The principal direction is perpendicular to the body surface of the fragment, and the second direction is almost in the plane of the axis of symmetry and the principal

normal, due to the weight of the rim points. Thus, the eigenvectors of the surface tensor can be used also for an initial positioning of the potsherd for further analysis.

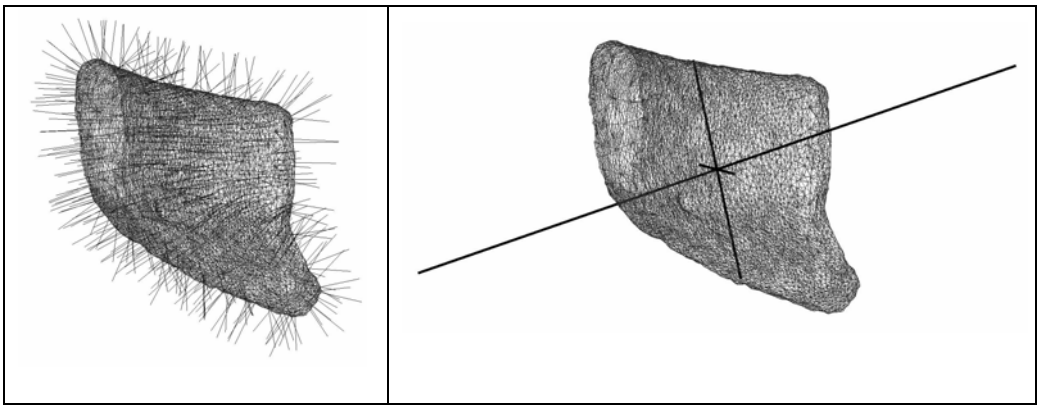

Figure 21: A typical potsherd from Tel Dor and its surface normal vectors (left). The thick lines in the right frame represent the directions of the surface tensor eigenvectors. Their length is proportional to the eigenvalues.

To improve on this rough approximation, one may repeat the computation, eliminating now the points on the surface with normal vectors which are approximately parallel to the principal direction obtained in the first computation. The main eigenvector of the resulting tensor defines better the direction normal to the rim or the base of the potsherd.

A.3 The mean thickness of a potsherd –

In the definition of the alignment quality parameter *Q* we use the thickness of the potsherds for normalization. Although the intuitive meaning of the term is clear, the computation of this parameter requires a precise definition.

We define the *local thickness* at a point P_1 (or P_2) - see figure 22 - along the profile as the distance between the point and the intersection of the *(ingoing) normals* N_1 (or N_2) with the profile Q_1 (or Q_2). This definition is useful when, locally, the profile consists of approximately parallel lines. However, there are sections in which the local thickness does not represent the true thickness of the vessel (e.g. P_2 - Q_2 in Figure 22). To rectify this problem we defined the *reverse normal* R_1 (or R_2) which is

the local normal at the intersection point (drawn in figure 22 as dotted lines from Q_1, Q_2). The *reverse normal* intersects the profile at the point F_1 (or F_2). The two normals approximately coincide when the profile consists of approximately (locally) parallel lines (N_1, R_1 in Figure 22). This is not the case when this condition is not satisfied (N_2, R_2). We defined the *reverse distance* which is the Euclidean distance between our original point (P_1 or P_2) and the reverse intersection point (F_1 and F_2).

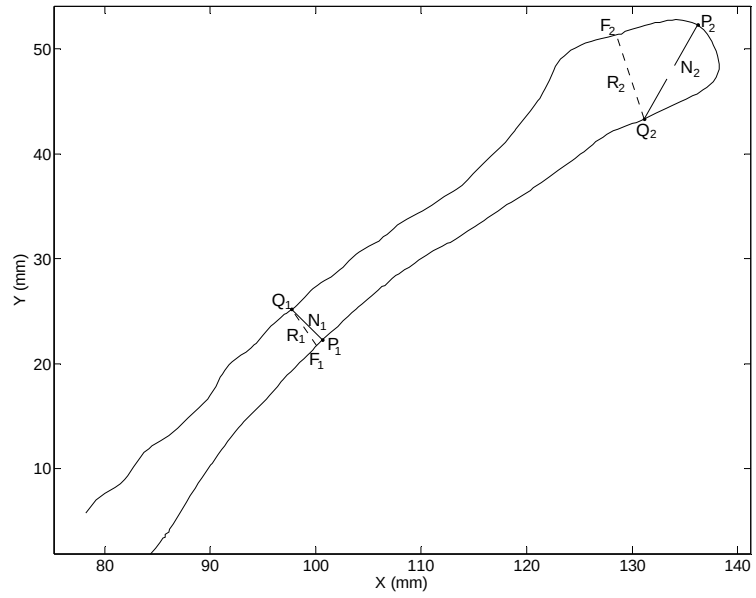

Figure 22: A profile of a bowl fragment from Kefar-Hananya where the points refer to in the text are marked.

To get a proper definition of the mean thickness, we consider only those points on the profile for which the *reverse distance* is less than a predetermine tolerance (typically 3mm), and compute their mean. Figure 23 (left) shows the distribution of the *reverse distance* along the profile shown in Figure 22. The threshold value of 3mm is marked as a dotted line. The points which contribute to the mean thickness are marked on the profile shown in Figure 23 (right).

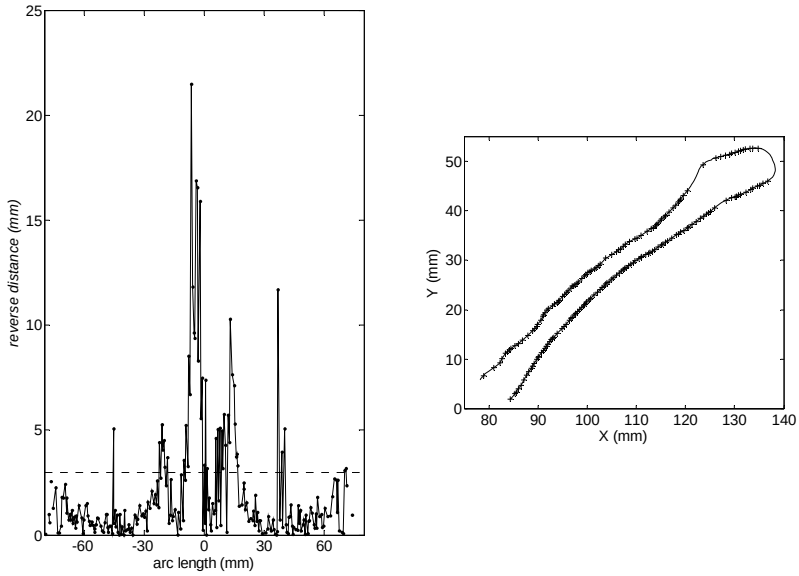

Figure 23: The distribution of the *reverse distance* along the profile of a bowl fragment (left), where all points with *reverse distance* lower than 3mm are highlighted at the right.

A.4 The sensitivity of Q to the positioning parameters -

As explained in Section III, the positioning algorithm varies four parameters $b_x, b_y, \theta, \varphi$, to find the shift and orientation of the axis of symmetry relative to a fixed reference coordinate system. The quality parameter Q is a function of these parameters and the optimal positioning is defined as the point in the four dimensional space where Q is minimal. In the present section we study the sensitivity of Q to the shift and orientation parameters in the vicinity of the minimum point.

The computations were carried out on a synthetic surface of revolution, created by turning a profile about its axis. A random, triangulated mesh of points is distributed on the surface to emulate the point cloud obtained from the scanner for real fragments. Finally, only a sixth of the entire circumference (which includes the rim) is used for the analysis, thus imitating a fragment.

The advantage of working with such a synthetic fragment is that it does not suffer from macroscopic or microscopic deformations, and the only source of "noise" is the finite mesh size. This way, the minimum value of Q (denoted by Q_0) is much

smaller than the value obtained for archaeological fragments. Therefore Figures 24-25 show Q/Q_0 rather than Q itself.

As can be seen from Figures 24-25, Q/Q_0 responds to variations of the shift and orientation parameters in a non uniform way: Keeping the orientation fixed, and shifting the symmetry axis along the principal normal of the fragment, (see Appendix *A*2), Q/Q_0 varies relatively slowly. On the other hand, when the axis is shifted perpendicularly to this direction, Q/Q_0 changes significantly.

The most conspicuous feature in Figure 24 is the narrow valley along the b_x-axis in which the parameter Q/Q_0 changes gradually, indicating that the uncertainty in the final value of b_x is maximal. To estimate it we note that to change Q/Q_0 from 1 to 2 one needs to change b_x by 0.66 mm, while the same change along the b_y-axis happens already after 0.054 mm. This value depends, of course, on the size of the fragment. Smaller potsherds will show even less sensitivity to shifts along the principal normal of the surface.

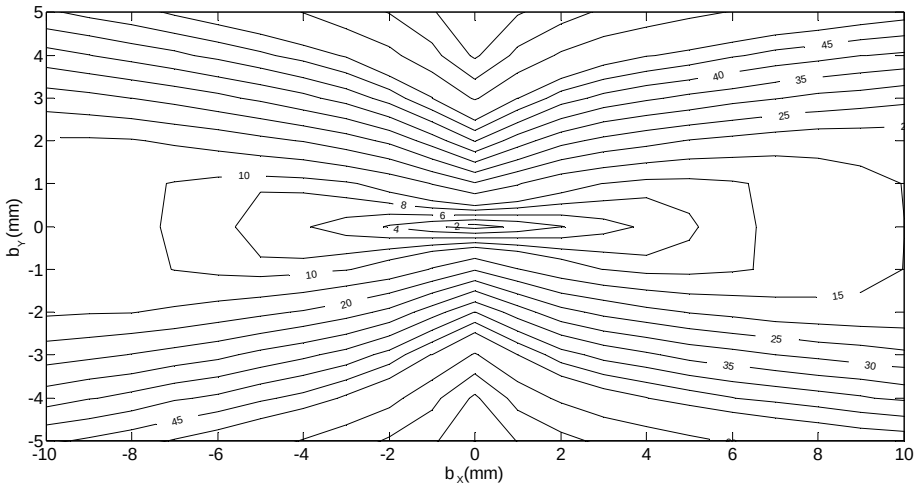

Figure 24: Topographic map of the quality parameter Q/Q_0 as a function of shifts of the symmetry axis in the neighborhood of the minimum. Note the narrow valley along the b_x-axis in which Q is changing slowly.

Tilting the rotation axis shows similar trend, where directing the axis towards the principal normal influences Q much slower than directing the axis in the perpendicular direction. Figure 25 illustrates this phenomenon in terms of the two orientation angles φ and θ, while $b_x = b_y = 0$. The computed Q/Q_0 is plotted as a topographic map in Figure 25.

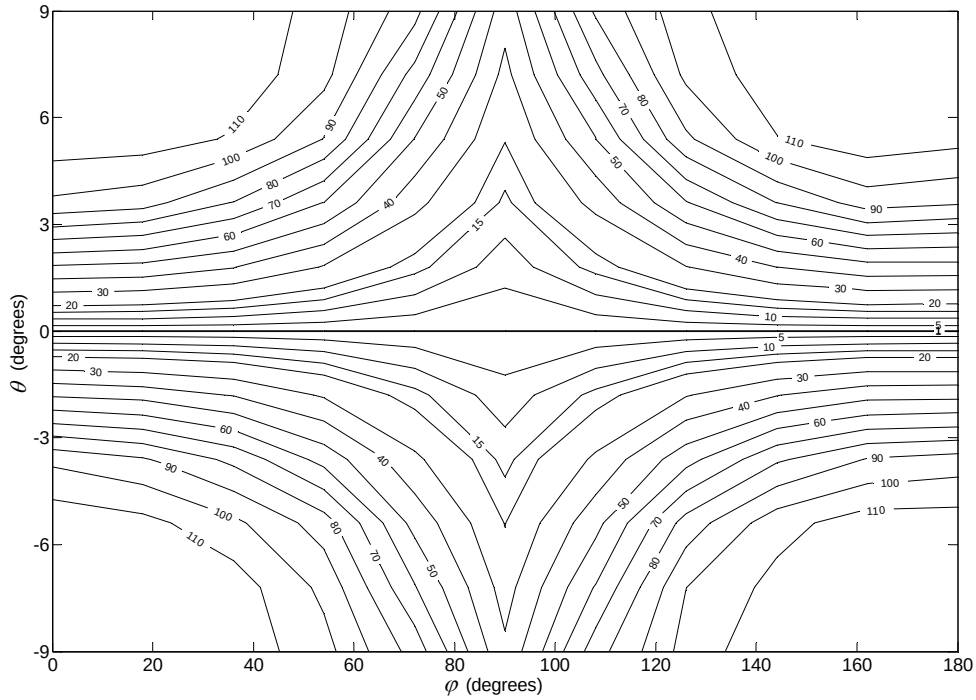

Figure 25: Topographic map of the quality parameter Q as a function of two rotation angles. Note that the two axes are not scaled.

Obviously, rotating by an angle φ without tilting ($\theta = 0$), has no effect on the quality parameter, since the projected profiles are identical. Moreover, a rotation by $\varphi = 90^o$ turns the principal normal of the fragment to be parallel to the y-axis, so further tilt of θ has minimal influence. This is the reason for the gradual vertical valley in the center of Figure 25. The steepest slope at the left and right of the figure occurs when θ changes without any rotation of φ (or when $\varphi = 180^o$), which orients

the symmetry axis in a direction perpendicular to the principal normal of the fragment.

In summary we can say that the quality parameter Q/Q_0 responds sensitively to any rotation or shift which is not confined to the plane defined by the principal normal and the true axis. Shifts within this plane also cause Q/Q_0 to increase, however, here the changes are more moderate, and their magnitude depends sensitively on the size of the fragment.

Bibliography

[1] D. Adan-Bayewitz, Common Pottery in Roman Galilee: A study of local trade, Bar-Ilan University Press, Ramat-Gan, Israel, 1993.

[2] K. Adler, M. Kampel, R. Kastler, M. Penz, R. Sablatnig, K. Schindler, S. Tosovic, Computer Aided Classification of Ceramics - Achievments and Problems. In: Proc. of 6th Intl. Workshop on Archaeology and Computers, Vienna, Austria, 2001.

[3] S. Ben Yacoub, C. Menard, Robust axis determination for rotational symmetric objects out of range data. In: W. Burger, M. Burge (Eds.), 21 th Workshop of the Oeagm, Hallstatt, Austria, 1997, pp. 197-202.

[4] Y. Cao, D. Mumford, Geometric Structure Estimation of Axially Symmetric Pots from Small Fragments, Proc. of Int. Conf. on Signal Processing, Pattern Recognition, and Applications, Crete, 2002. (2001).

[5] C. Commenge-Pellerin, La Potterie d'Abou Matar et de l'Ouadi Zoumeili (Beersheva) au IV'e mill'enaire avant l'e're chr'etienne, Association Pal'eorient, Paris, 1987.

[6] C. Commenge-Pellerin, La Potterie de Safadi(Beersheva) au IV'e mill'enaire avant l'e're chr'etienne, Association Pal'eorient, Paris, 1990.

[7] P. Dolmazon, http://www.dolmazon.de/profilograph_e.htm. In, 2007.

[8] Y. Garfinkel, Neolithic and Chalcolithic Pottery of the Southern Levant - Qedem 39, The Hebrew University of Jerusalem, Jerusalem, 1999.

[9] A. Gilboa, A. Karasik, I. Sharon, U. Smilansky, Towards computerized typology and classification of ceramics, Journal of Archaeological Science 31 (2004) 681-694.

[10] A. Gilboa, I. Sharon, An archaeological contribution to the early Iron Age chronological debate: Alternative chronologies for Phoenicia and their effects on the Levant, Cyprus and Greece, Bulletin of the American Schools of Oriental Research 332 (2003) 7-80.

[11] N.A.J. Griffiths, C. Wilson, Drawing Archaeological Finds: a handbook., Archetype Publications, London, 1991.

[12] R. Halir, An automatic estimation of the axis of rotation of fragments of archaeological pottery: A multi-step model-based approach. In: V. Skala (Ed.),

Proc. of the 7th International Conference in Central Europe on Computer Graphics, Visualization and Interactive Digital Media (WSCG'99), 1999.

[13] R. Halir, J. Flusser, Estimation of the axis of rotation of fragments of archaeological pottery. In: W. Burger, M. Burge (Eds.), 21 th Workshop of the Oeagm, Hallstatt, Austria, 1997, pp. 175-184.

[14] C. Horr, D. Brunner, G. Brunnett, Feature Extraction on Axially Symmetric Pottery for Hierarchical Classification, Computer-Aided Design & Applications 4 (2007).

[15] M. Joukowsky, A complete manual of field archaeology, Prentice-Hall, Englewood Cliffs, N.J., 1980.

[16] M. Kampel, H. Mara, R. Sablatnig, Robust 3D Reconstruction of Archaeological Pottery based on Concentric Circular Rillss. In: N. Magnenat-Thalmann, J.H. Rindel (Eds.), Proc. of the 6th International Workshop on Image Analysis for Multimedia Interactive Services (WIAMIS'05), Montreux, Switzerland, 2005, pp. 14-20.

[17] M. Kampel, R. Sablatnig, Rule based system for archaeological pottery classification, Pattern Recognition Letters (in press).

[18] A. Karasik, L. Bitton, A. Gilboa, I. Sharon, U. Smilansky, Quantitative Measures of the Uniformity of Ceramics, Computers Applications and Quantitative Methods in Archaeology (CAA 2004) (In press).

[19] A. Karasik, H. Mara, R. Sablatnig, I. Sharon, U. Smilansky, Measuring deformations of wheel-produced ceramics using high resolution 3D reconstructions, Computers Applications and Quantitative Methods in Archaeology - CAA 2005 (In press).

[20] F. Leymarie, D. Cooper, M.S. Joukowsky, B. Kimia, D. Laidlaw, D. Mumford, E. Vote, The SHAPE Lab. - New Technology and Software for Archaeologists. In: Z. Stancic, T. Veljanovski (Eds.), Computing Archaeology for Understanding the Past CAA2000. Computer Applications and Quantitative Methods in Archaeology. BAR International Series 931,, Archaeopress, Oxford, 2001, pp. 79-89.

[21] H. Mara, Documentation of Rotationally Symmetric Archaeological Finds by 3D shape Estimation. In: Institute of Computer Aided Automation, Vol. Ph.D., Vienna University of Technology, Vienna, 2006.

[22] H. Mara, R. Sablatnig, Semiautomatic and Automatic Profile Generation for Archaeological Fragments. In: A. Hanbury, H. Bischof (Eds.), Proc. of 10th Computer Vision Winter Workshop (CVWW05), 2005, pp. 123-134.

[23] H. Mara, R. Sablatnig, A. Karasik, U. Smilansky, The Uniformity of Wheel Produced Pottery Deduced from 3D Image Processing and Scanning. In: W. Burger, J. Scharinger (Eds.), Digital Imaging in Media and Education, Proc. of the 28th Workshop of the Austrian Association for Pattern Recognition (OAGM), Hagenberg, Austria, 2004, pp. 197-204.

[24] C. Orton, P. Tyres, A. Vince, Pottery in Archaeology, University Press, Cambridge, 1993.

[25] J. Perrot, D. Ladiray, Tombes `a Ossuaires de la R´egion Cˆoti`ere Palestinienne au IVe mill´enaire avant l'Ere Chr´etienne, Association Pal´eorient, Paris, 1980.

[26] J. Pobelome, J. van den Brandt, B. Michiels, G. Evesever, R. Degeest, M. Walkens, Manual Drawing versus Automated Recording of Ceramics. In: M. Walkens (Ed.), Sagalasos IV Acta Archaeologica Lovaniensia Monographiae 9, Leuven, 1997, pp. 533-538.

[27] H. Pottmann, M. Peternell, B. Ravani, An Introduction to line Geometry with Applications, Computer Aided Design 31 (1999) 3-16.
[28] A. Razdan, D. Liu, M. Bae, M. Zhu, G. Farin, Using Geometric Modeling for Archiving and Searching 3D Archaeological Vessels. In: International Conference on Imaging Science, Systems, and Technology CISST 2001, Las-Vegas, 2001.
[29] P.M. Rice, Pottery Analysis: A Sourcebook, University Press, Chicago, 1987.
[30] V. Roux, A Dynamic Systems Framework for Studying Technological Change: Application to the Emergence of the Potter's Wheel in the Southern Levant, Journal of Archaeological Method and Theory 10: 1-30 (2003).
[31] V. Roux, M.A. Courty, Identifying Social Entities at a Macro-Regional Level: Chalcolithic Ceramics of South Levant as a Case Study. In: L.S.A.D. Bosquet, R. Martineau (Eds.), Pottery Manufacturing Processes: Reconstitution and Interpretation, BAR international Series 1349, 2005, pp. 201-214.
[32] R. Sablatnig, C. Menard, Computer based Acquisition of Archaeological Finds: The First Step Towards Automatic Classification. In: P. Moscati, S. Mariotti (Eds.), the 3rd International Symposium on Computing and Archaeology, Vol. 1, Rome, 1996, pp. 429-446.
[33] I. Saragusti, A. Karasik, I. Sharon, U. Smilansky, Quantitative analysis of shape attributes based on contours and section profiles in archaeological research, Journal of Archaeological Science 32 (2005) 841-853.
[34] U. Schurmans, A. Razdan, A. Simon, P. McCartney, M. Marzke, D. Van Alfen, G. Jones, J. Rowe, G. Farin, D. Collins, M. Zhu, D. Liu, M. Bae, Advances in Geometric Modeling and Feature Extraction on Pots, Rocks and Bones for Representation and Query via the Internet. In: Computer Applications in Archaeology (CAA) 2001, Visby Sweden, 2001.
[35] I. Sharon, The 2004 Season at Dor: A Personal Assessment and Preliminary Report. In, http://micro5.mscc.huji.ac.il/~dor/2004report.htm, 2004.
[36] E. Stern, J. Berg, A. Gilboa, B. Guz-Zilberstein, A. Raban, R. Rosenthal-Heginbottom, I. Sharon, Excavations at Dor, Final Report, Volume I B, Areas A and C:The Finds (Qedem Reports 2), Institute of Archaeology of the Hebrew University, Jerusalem, 1995.
[37] F. Yao, G. Shao, Detection of 3D symmetry axis from fragments of a broken pottery bowl, Acoustics, Speech, and Signal Processing, 2003. Proceedings. (ICASSP '03). 3 (2003) 505-508.